IET Nanobiotechnology

Research Article

IET Journals
The Institution of Engineering and Technology

Synthesis, radiolabelling, and biological assessment of folic acid-conjugated G-3 ^{99m}Tc-dendrimer as the breast cancer molecular imaging agent

ISSN 1751-8741
Received on 12th May 2020
Revised 24th July 2020
Accepted on 28th July 2020
E-First on 1st September 2020
doi: 10.1049/iet-nbt.2020.0176
www.ietdl.org

Saedeh Zamani[1], Mehdi Shafeie-Ardestani[1], Ahmad Bitarafan-Rajabi[2,3,4], Ali Khalaj[1], Omid Sabzevari[5] ✉

[1]*Department of Radiopharmacy, Faculty of Pharmacy, Tehran University of Medical Sciences, Tehran, Iran*
[2]*Cardiovascular Interventional Research Center, Iran University of Medical Sciences, Tehran, Iran*
[3]*Rajaie Cardiovascular Medical and Research Center, Iran University of Medical Sciences, Tehran, Iran*
[4]*Echocardiography Research Center, Iran University of Medical Sciences, Tehran, Iran*
[5]*Department of Toxicology and Pharmacology, Faculty of Pharmacy, and Toxicology and Poisoning Research Centre, Tehran University of Medical Sciences, Tehran, Iran*
✉ *E-mail: omid@sina.tums.ac.ir*

Abstract: Hence, in this study, the authors aimed to develop a dendrimer-based imaging agent comprised of poly(ethylene glycol) (PEG)-citrate, technetium-99 m (^{99m}Tc), and folic acid. The dendrimer-G3 was synthesised and conjugated with folic acid, which confirmed by Fourier transform infrared, proton nuclear magnetic resonance, dynamic light scattering, and transition electron microscopy. 2,3-bis-(2-methoxy-4-nitro-5-sulfophenyl)-2H-Tetrazolium-5-Carboxanilide cytotoxicity assay kit was used to measure the cellular toxicity of dendrimer. Imaging and biodistribution studies were conducted on the mice bearing tumour. The results showed that the fabricated dendrimer-G3 has a size of 90 ± 3 nm, which was increased to 100 ± 4 nm following the conjugation with folic acid. The radiostablity investigation showed that the fabricated dendrimers were stable in the human serum at various times. Toxicity assessment confirmed no cellular toxicity against HEK-293 cells at 0.25, 0.5, 1, 2, 4, and 8 mg/µl concentrations. The in vivo studies demonstrated that the synthesised dendrimers were able to provide a bright SPECT image applicable for tumour detection. In conclusion, the authors' study documented the positive aspects of PEG-citrate dendrimer conjugated with folic acid as the SPECT contrast agent for breast cancer detection.

1 Introduction

Breast cancer is a term that refers to the out of control and rapid growth/division of abnormal breast cells, which overcrowd normal cells [1]. According to the National Center for Health Statistics (NCHS) reports breast cancer is the most common cancer in women, and about 1 in 8 US women (about 12.4%) will develop invasive breast cancer throughout her lifetime [2]. Moreover, 63,960 new cases of non-invasive (in situ) breast cancer are expected to be diagnosed, along with 266,120 new cases of invasive breast cancer. Interestingly, breast cancer is not solely women-specific and men can get it, too [3, 4]. It is estimated about 2550 new cases of invasive breast cancer in men in 2018 and a man's lifetime risk of breast cancer is about 1 in 1000 [2, 5–7]. The breast cancer incidence was reported in 7582 cases (23% of total cancers in women) in 2009 in Iranian women [8].

The success of cancer treatment and survival of a cancer patient depends significantly on the early detection of cancer cells. The current detecting methods for breast cancer are digital mammography [9, 10], computer-aided detection (CAD) [11, 12], ultrasound imaging [13], and magnetic resonance imaging (MRI) [14, 15]. Moreover, there are some other imaging technologies under development for breast cancer detection, including positron emission tomography (PET) [16, 17], single-photon emission computed tomography (SPECT) [18], and SPECT/CT imaging. Despite their versatility in cancer detection, they are not very powerful methods, in the traditional form, when it comes to cancer detection at very early stages. Researchers are working on diagnostic methods to detect distinctive 'molecular signatures' of a pre-malignant or malignant breast tumour at the earliest stage. This can be done by working on the improvements of current techniques and/or new imaging modalities of cancer detection [19, 20].

Molecular imaging (MI) is a promising biomedical detecting approach that enables the quantification, characterisation, and visualisation of biologic processes taking place at the cellular and subcellular levels within intact living subjects, including patients [21, 22]. Generally, MI comprised two main parts, a sophisticated imaging modality and a selective and specific contrast agent. While the conventional imaging modalities, such as ultrasound, computed tomography (CT), and X-rays, provide pictures of physical structure, MI offers the ability to measure chemical and biological processes at the cellular and subcellular levels [23]. SPECT/CT technique is a sophisticated imaging modality applicable in MI, which provides the ability to capture two essential and complementary images and combine results at the same time [24]. The current and usual contrast agents for SPECT is ^{99m}Tc based contrast agents, which suffer from low specificity. Nanomaterials and nanotechnology can overcome the drawbacks of the current contrast agents due to their promising properties.

Nanotechnology is enabling approaches dealing with subjects at the size scale lower than 100 nm [25, 26]. Nanotechnology and nanomaterials are involving in various fields of medical sciences and technology such as drug delivery [27–29], tissue engineering [30–32], wound dressing [33–35], cancer detection and therapy [36, 37]. Dendrimers are a versatile class of polymeric nanostructures known as highly branched, globular, nanosized, highly monodispersed, multifunctional, and highly symmetrical polymeric three-dimensional (3D) structures [38–40]. Dendrimers offer a wide range of advantages over linear polymers such as controllable 'surface' functionalities, ability to conjugate with various imaging agents, targeting ligands, and therapeutic payloads, which make these structures suitable for cancer imaging and therapy (the theranostic agent). Despite these promising futures, the current dendrimers are cytotoxic due to the high cationic charge density in the periphery, which disrupts cell membrane integrity under interaction with negatively charged membrane phospholipids [41]. Alternatively, using biocompatible polymers such as poly(ethylene glycol) (PEG) and introducing

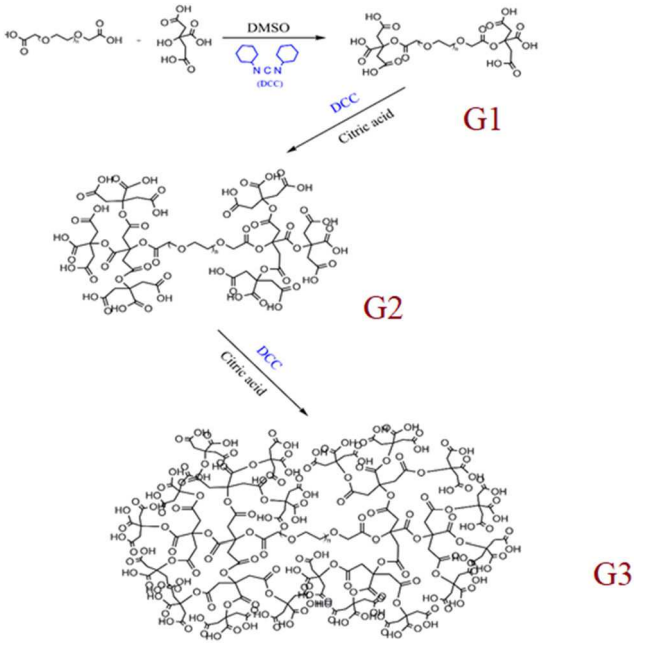

Fig. 1 *PEG-citrate dendrimers fabrication process. PEG diacid 600 was activated by DCC in DMSO-d6, then the monomers (citric acid) was added to the solution to generate G1 dendrimer. These processes were repeated to synthesised G2 and G3 dendrimers*

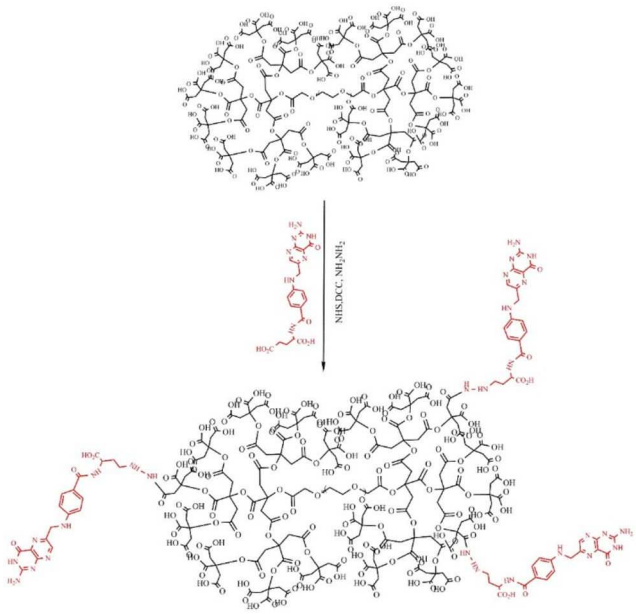

Fig. 2 *Conjugation of the synthesised dendrimer with folic acid. The synthesised dendrimers were activated by DCC and reacted folic acid. Amid bonding was formed between amine functional groups folic acid and carboxylic groups of the dendrimer*

anionic functional groups such as citric acid can eliminate the toxicity concern and improve the biocompatibility [42–44]. The generation of dendrimers impacts the physicochemical and the biological properties as the higher generations provide greater peripheral functional groups. These functional groups are essential for conjugating a higher amount of radionuclides, as well as the targeting agent. In this circumstance, G3 dendrimers provide more strength and a more precise signal than G2. Well-designed and functionalised dendrimers with cancer-specific biomarkers, which specifically target cancer cells, are promising to eliminate the non-specific toxicity and promote treatment efficacy.

An effective breast cancer imaging modality must exploit a targeting agent providing selectivity and specificity. Breast cancer cells overexpress folate receptors on their surface and use them as their major and distinct route for folate entry into the cell. Overexpression of the folate receptors was associated with basal-like breast cancer cells. Various studies have been conducted to breast cancer cells imaging using folic acid as the targeting agents [45–47]. Accordingly, the purpose of the present study was to fabricate a breast cancer imaging agent based on PEG-citrate dendrimers decorated with ^{99m}Tc as the imaging agent and folic acid as the targeting agent.

This study is the first report on the third generation of citric acid-based dendrimers, which is applicable in biomedical applications, especially in nuclear medicine.

2 Materials and methods

2.1 Chemicals

PEG diacid 600, 2,3-bis-(2-methoxy-4-nitro-5-sulfophenyl)-2H-Tetrazolium-5-Carboxanilide (XTT), and N,N′-dicyclohexylcarbodiimide (DCC) were purchased from Sigma-Aldrich (St. Louis, USA). Dimethyl sulfoxide (DMSO), folic acid, hydrochloric acid (HCl), citric acid, adipic acid dihydrazide (ADH), and trichloroacetic acid were obtained from Merck (Darmstadt, Germany). Trypsin/EDTA, penicillin, streptomycin, Dulbecco's modified Eagle's medium: nutrient mixture F-12 (DMEM/F12), and foetal bovine serum (FBS) were purchased from Gibco, BRL (Eggenstein, Germany). Female nude mice and HEK-293 cell lines were obtained from the Pasteur Institute (Iran). Ketamine and Xylazine were obtained from Alfasan (Woerden, the Netherlands).

2.2 Dendrimers fabrication and conjugation

First off, dendrimer-G2 (second generation) was synthesised based on the previous studies [48]. Briefly, PEG diacid 600 was dissolved in DMSO and DCC in dimethyl sulfoxide-d6 (DMSO-d6) was added as the activator, and the solution kept at room temperature under stirrer. In the next step, the monomers (citric acid) were added to the solution and stirred for 24 h at room temperature. Unreacted DCC was precipitated using distilled water and the product was purified by dialysis bag. The synthesised dendrimer-G1 was activated using DCC in DMSO-d6 and reacted with citric acid as the monomer under stirrer for 24 h at room temperature to produce dendrimer-G2. The resulted products were purified using a dialysis bag after precipitation of unreacted DCC by distilled water. This process was repeated one more time to produce dendrimer-G3 (Fig. 1). In the next step, ADH was used to optimise the surface of the synthesised dendrimer-G3 and induce NH_2 functional groups. Briefly, 5 ml DMSO containing 150 mg ADH and 1 g DCC was added to the solution of dendrimer-G3 and kept for 4 days under stirrer. The purification of the products was done based on the mentioned process.

In the next step, folic acid was conjugated to the synthesised dendrimer-G3, as described in Fig. 2. Briefly, the prepared dendrimer-G3 (0.05 g) was activated by 0.02 g DCC in 10 ml DMSO under stirrer for 30 m. The activated dendrimers were reacted with 0.02 g folic acid under stirrer for 48 h at room temperature to react completely with the carboxylate terminal groups of the dendrimer. The protecting groups of the reaction products were removed by using HCl (0.1%). Afterwards, distilled water was added to the reaction mixture to precipitate DCU and the final products were purified using a dialysis bag (cut-off 500–1000 Da).

2.3 ^{99m}Tc radiolabelling of dendrimer–folate conjugate

The radiolabelling was conducted based on the previously described method. In this regard, 10 mg of lyophilised nanocomplex was dissolved in 2 ml DD water, then 0.4 ml antioxidant agent (5 mg/ml ascorbic acid) and 0.3 ml tin chloride solution (1 mg/ml) were added to the solution. In the next step, the pH of the solution was adjusted to be 8 and the resulted solution lyophilised using a freeze drier (Telstar, Terrassa, Spain) for 24 h at −54°C. In the final stage, 370 MBq $^{99m}TcO_4$ obtained from ^{99}Mo/

^{99m}Tc generator was incubated with the dendrimers at room temperature for 10 min.

2.4 Characterisation

The infrared spectrum of the fabricated samples was recorded using a Perkin Elmer Spectrum BX-II spectrometer (PerkinElmer, Inc., Waltham, MA, USA). ^{1}H-NMR spectra of the synthesised and conjugated dendrimers were massacred by a Bruker 500 MHz instrument (Billerica, Massachusetts, Germany) and DMSO-d6 was used as the solvent. The hydrodynamic size of the particles was measured based on the dynamic light scattering (DLS) method using Malvern nano-zs (Malvern Instruments Ltd., Malvern, Worcestershire, UK). The morphology of the dendrimers was observed via atomic force microscopy (AFM, JPK Nanowizard II, Germany) and transmission electron microscope (TEM, JEOL JEM-2100, Japan).

2.5 Radiochemical purity assessment

For the radiochemical purities (RCPs) measurement of the dendrimers, the solid phase and the mobile phase were Whatman paper and saline and acetone/methanol (1: 1), respectively. This method is based on the distinct movement of the radiolabelled dendrimer, free pertechnetate, and $^{99m}TcO_2$ on the paper under the flow of the mobile phase. 5 µl of the specimen was spotted at the one side of the paper and after the segmentation of the samples, the radioactivity of each segment was recorded by a γ well-type counter. By applying saline, free pertechnetate and the radiolabelled dendrimer moved along with the solvent, while $^{99m}TcO_2$ was fixed at the spotted site. On the other hand, using acetone/methanol, free pertechnetate moved along the solvent, while $^{99m}TcO_2$ and the radiolabelled dendrimer was fixed. In this regard, (1) was used to calculate RCP value

$$\text{RCP} = 100 - (\text{free pertechnetate} - {}^{99m}TcO_2) \quad (1)$$

2.6 Stability test

The stability of the nanoconjugates was evaluated in human serum at 37°C and a PBS solution at room temperature. The nanocomplex (300 µl) was incubated in human serum (600 µl) and PBS (600 µl) and at predetermined time points, 100 µl trichloroacetic acid (10%) added to the solutions. Finally, the serum proteins were removed via centrifugation and the stability of the conjugates measured via chromatography.

2.7 Cell toxicity assessment

The toxicity of the synthesised dendrimers was evaluated on the HEK-293 cell line using the XTT assay kit. XTT assay is a colorimetric assay that measures the viability of cells based on metabolic activity. The cells were cultured in DMEM/F12 supplemented with FBS 10% (v/v), penicillin (100 unit/ml), and streptomycin (100 µg/ml). The number of 10,000 cells/100 µl culture media was seeded into the 96-well culture plate and incubated for 24 h, then 50 µl of the nanoconjugates with concentrations of 0.25, 0.5, 1, 2, 4, and 8 mg/ml were added and incubated at 37°C, 5% CO_2, and the humidity of 90% for 24 and 48 h. At the end of each time point, 25 µL of the XTT/ N-methylphenazonium methyl sulphate (PMS) (50:1 µl) was added to each well, incubated for 2 h, and the absorbance was read at a wavelength of 450 nm using a spectrophotometer. The obtained results were compared with the control group (untreated cells).

2.8 Animal study

The animal studies were conducted on female nude mice (20–28 g) according to the instruction of the ethics committee of Tehran University of Medical Sciences (number IR.Tums.REC.1394.1509). The tumour induction was done according to the previously established protocol [48, 49] as the following. Each nude mouse was subcutaneously injected in the right flank with 1×10^6 HEK-293 cells suspended in 100 µl PBS solution.

2.8.1 Scintigraphic images: The animals were anaesthetised by intraperitoneal injection of ketamine 100 mg/xylazine 10 mg/kg of body weight. ^{99m}Tc-conjugated dendrimer (3.7 MBq) was injected through the tail vein into nude mice bearing the tumour. The imaging was conducted using SPECT/CT imaging system (Siemens, SimbiaT2 equipped with low energy high-resolution collimators) at 3 h after injection ($n = 3$). The anaesthetised animal was horizontally placed under the imaging system, and the images were acquired using a 256×256 matrix size with a 20% energy window set at 140 keV.

2.8.2 Biodistribution studies: ^{99m}Tc-conjugated dendrimer (3.7 MBq) was injected into the animals through the tail vein under anaesthesia. The animals were euthanised at different time intervals (30, 60, 90, and 120 min), and the intended tissues (spleen, liver, cortical bone, and kidney) were excised, weighed, and counted. Calibrated gamma counter was used to measure the radioactivity in different tissues and organs and the values calculated as the percent of the injected dose per gram of the tissue divided by total activities.

2.9 Statistical analysis

Prism 5 and Excel software (Microsoft Office 2013) were used for statistical data analysis. The obtained results were quantitatively analysed via the one-way analysis of variance (ANOVA) followed by Tukey's test. The statistically significance level was set at $p < 0.05$.

3 Results and discussion

3.1 Size, zeta potential, and surface morphology of the conjugate

The synthesis, conjugation, and radiolabelling of the dendrimers were conducted based on Figs. 1 and 2. The structure and composition of the synthesised dendrimers were determined by ^{1}H NMR spectroscopy in DMSO-d6, as shown in Fig. 3. The results showed the observed peaks around 2.7 ($2J = 15.5$ Hz, 2 h), 3.5 (*t*, $3J = 5$ Hz, 2 h), and 5.02 (*s*, 2 h) in Fig. 3*a* are related to the CH_2COOH functional group of citric acid, OCH_2CH_2 and OCH_2CO functional groups of PEG, respectively. These peaks confirmed the presence of citric acid and PEG in the synthesised dendrimer-G2.

According to Fig. 3*b*, it can be concluded the formation of dendrimer-G3. The results showed that the obtained and calculated-theoretical ratio of citric acid-H to PEG-H were 0.77 and 0.75, respectively. The peaks observed at 2.3–2.8 ppm are corresponding to citric acid-H and the peaks around 3.5 ppm to PEG-CH_2. Moreover, the weak peak at 4.17 ppm is related to PEG-single H. The peaks related to citric acid and PEG are sharper in G3 dendrimers and these significant differences between the citric acid and PEG peaks in dendrimer-G2 and dendrimer-G2 indicated the conversion of G2 to G3. The formation of the dendrimers and the conjugation with folic acid were further evaluated by LC-MS spectroscopy and the results are presented in Fig. 4.

The peak around 306 m/z is attributed to the fragmentation of a citric acid attached to the second citric acid and a repetitive unit of PEG. The peak located at around 512 is related to five repetitive units of PEG conjugated to the citric acid molecules, and the peak around 696 m/z showed seven repetitive unite of PEG along with two citric acid molecules. These peaks confirmed the conjugation of citric acid molecules with each other from the terminal carboxylic acid groups and the attachment of them with PEG molecules, which are completely matched with the intended structures of the citrate-PEG dendrimer. The higher intensity of these peaks observed in Fig. 4*b* clearly indicates the conversion of G2-dendrimers to G3-dendrimers. Fig. 4*c* also confirmed the conjugation of the dendrimers with folic acid.

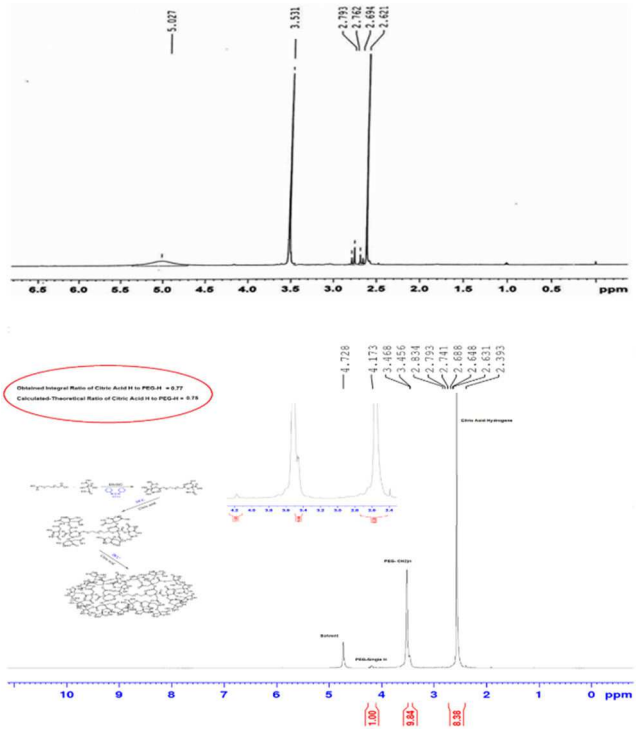

Fig. 3 *^{1}H NMR (500 MH_Z) spectra of*
(a) Dendrimer-G2, ***(b)*** Dendrimer-G3. Peaks around 2.7 ($2J = 15.5$ Hz, 2 h), 3.5 (*t*, $3J = 5$ Hz, 2 h), and 5.02 (s, 2 h) in Fig. 3*a* are related to the CH_2COOH functional group of citric acid, OCH_2CH_2 and OCH_2CO functional groups of PEG, respectively

FTIR spectroscopy was used to assess the synthesis and the conjugation processes of the dendrimers, and the results are shown in Fig. 5. The peak located at 1232 cm^{-1} is related to the C–O groups of ester bonding between terminal citric acid of dendrimer-G2 and citric acid monomers indicating the formation of dendrimer-G3. The peak around 1726 cm^{-1} is attributed to C = O groups of terminal citric acid and also indicated the formation of ester bonding. Moreover, C–O functional groups of PEG can be seen at 1084 cm^{-1}. The peaks around 3500 cm^{-1} also are related to the OH functional groups of citric acid. Moreover, stretching vibration of the C–O functional groups can be observed around 2925 cm^{-1}. As shown in Fig. 5, the NH peak of dendrimer-G3 (3390 cm^{-1}) shifted to 3433 cm^{-1} in dendrimer-G3-folic acid, indicating the formation of an amide bond between the carboxylic groups of folic acid and the terminal amine groups of dendrimer-G3. Chandrasekar *et al.* [50] showed that the shift in the position of the NH group could be attributed to the formation of amide bonds between folic acid and PEG.

The morphology of the synthesised dendrimers was visualised by TEM imaging (Fig. 6) and the size measured using Image J software. The TEM images showed that the synthesised dendrimers had a partially spherical shape with a diameter of 90 ± 3 nm for dendrimer-G3 and 100 ± 4 nm for folic acid-conjugated dendrimer-G3. These observations were consistent with DLS data, which showed that the hydrodynamic diameter of dendrimer-G3 was 115 nm with a poly disparity index (PDI) of 0.3 and these values for folic acid-conjugated dendrimer-G3 were 121 nm and 0.2, respectively. Moreover, the zeta potentials of dendrimer-G3 and dendrimer-G3-folic acid were −9.8 and −7.6 mV, respectively.

3.2 Stability test results

The stability of the fabricated nanocomplexes in the human body on the way to reach the target site is a vital requirement for effective molecular imaging. Serum protein adsorption around the nanocomplexes is the first event once the nanocomplexes are injected into the blood. This protein adsorption is called a protein corona formation, which is a critical and determinant factor. Inappropriate protein corona suppresses long term blood

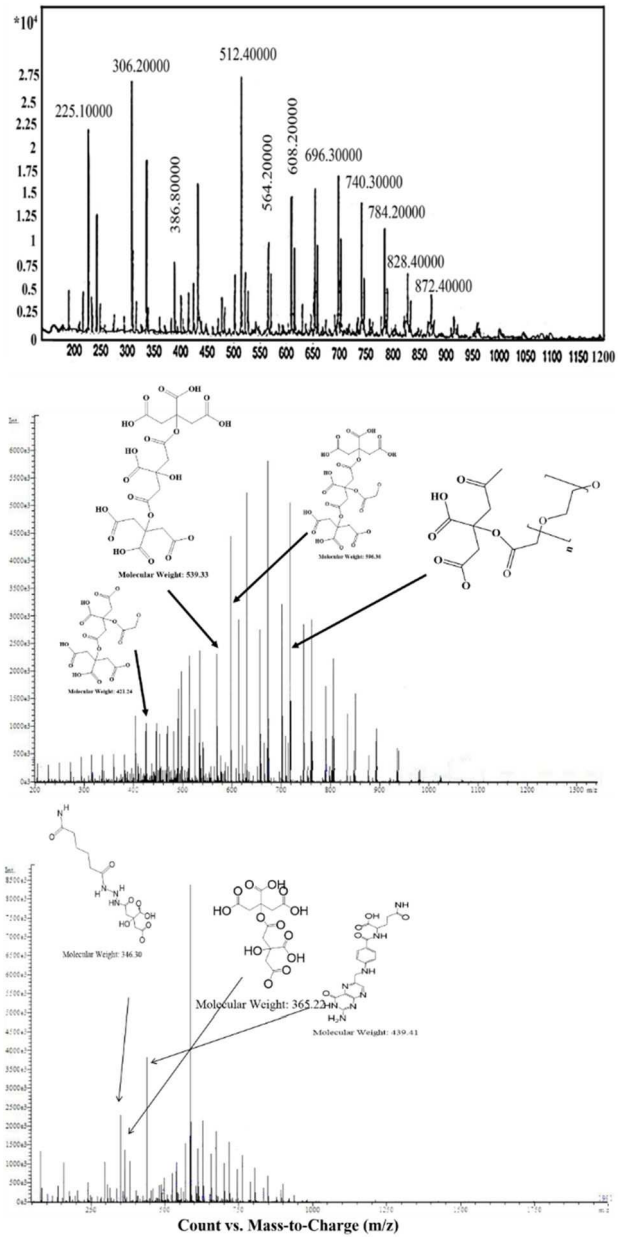

Fig. 4 *LC-MS spectroscopy of*
(a) Dendrimer-G2, ***(b)*** Dendrimer-G3, ***(c)*** Dendrimer-G3-folic acid. The peak around 306 m/z indicates the fragmentation of a citric acid attached to the second citric acid and a repetitive unit of PEG. The peak located at around 512 represents five repetitive units of PEG conjugated to the citric acid molecules and the peak around 696 m/z showed seven repetitive unite of PEG along with two citric acid molecules

circulation time, as well as the efficacy of the administrated nanocomplexes. The stability of the synthesised ^{99m}Tc-radiolabeled dendrimers was evaluated in human serum and PBS solution for 24 h.

As shown in Fig. 7, the nanoconjugates had acceptable stability in both serum and PBS and loss <15% of the radioactivity up to 24 h. These findings revealed that the ^{99m}Tc-radiolabelled dendrimers were suitable imaging in heterogeneous media such as human serum.

3.3 Toxicity results

The toxicity assessment was conducted on HEK-293 cells for the synthesised dendrimers at 0.25, 0.5, 1, 2, 4, and 8 mg/µl concentration (Fig. 8). The results implied that the synthesised ^{99m}Tc nanoconjugate did not induce any significant toxicity even at the highest concentration (8 mg/µl) for 24 h.

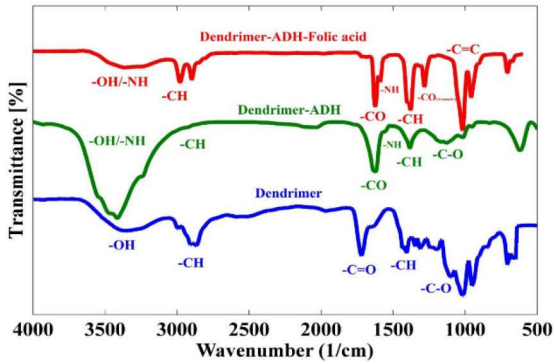

Fig. 5 *FTIR spectrum of the synthesised dendrimers. The peak located at 1232 cm^{-1} indicates the formation of dendrimer-G3. The peak around 1726 cm^{-1} is attributed to C = O groups of terminal citric acid. The peak around 1084 cm^{-1} is related to the C–O functional groups of PEG. The peaks around 3500 cm^{-1} also are related to the OH functional groups of citric acid*

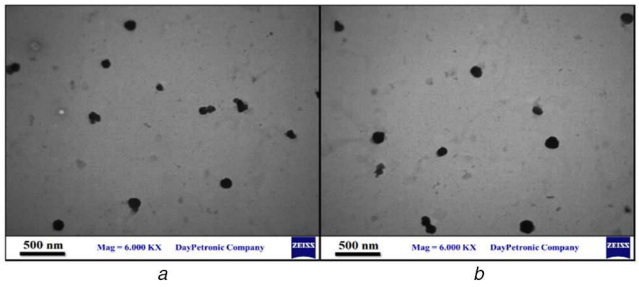

a *b*

Fig. 6 *TEM micrographs of*
(a) Dendrimer-G3, ***(b)*** Dendrimer-G3-folic acid. The synthesised dendrimers have a partially spherical shape

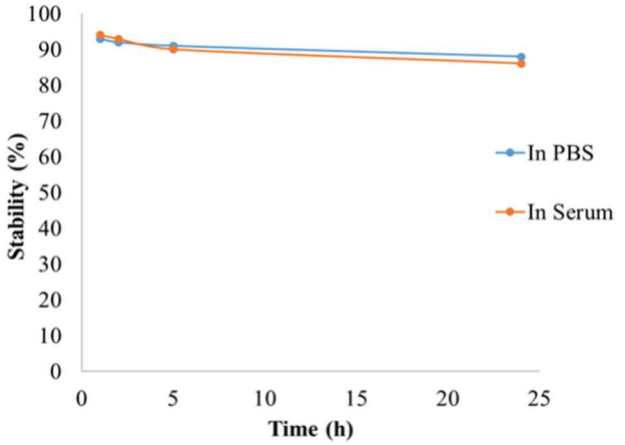

Fig. 7 *In vitro stability of ^{99m}Tc nanoconjugate complex in human serum at 37°C and PBS at room temperature during 24 h. PBS, phosphate-buffered saline*

3.4 Scintigraphic images and biodistribution studies

SPECT scan was acquired from mice bearing the tumour to evaluate the efficacy of the targeting approach, as well as and the biodistribution. Fig. 9 indicates the accumulation of targeted dendrimers 60 min after injecting 3.7 MBq of radiolabelled-conjugated-dendrimer.

As shown in Fig. 9, the conjugated dendrimers were accumulated in the tumour site 60 min post-injection. The acquired image clearly indicates that the ^{99m}Tc radiolabelled dendrimers conjugated with folic acid provide a bright SPECT signal in vivo. Moreover, the further accumulation of the synthesised dendrimers was assessed with biodistribution evaluation.

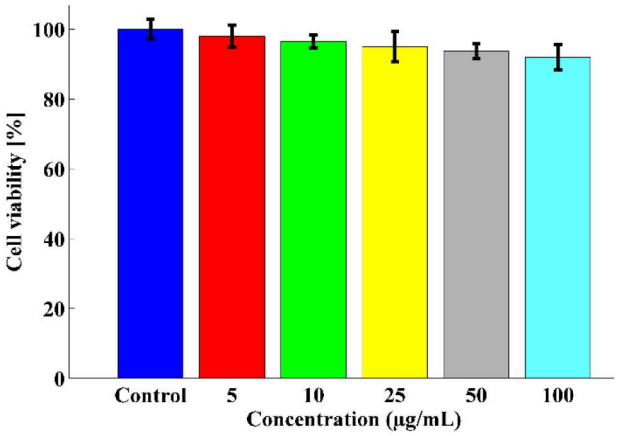

Fig. 8 *Cell viability of HEK-293 cells under incubation with the synthesised nanocomplex at 24 h measured by the XTT assay kit. There is an inverse relationship between the concentration of nanocomplex and cell viability*

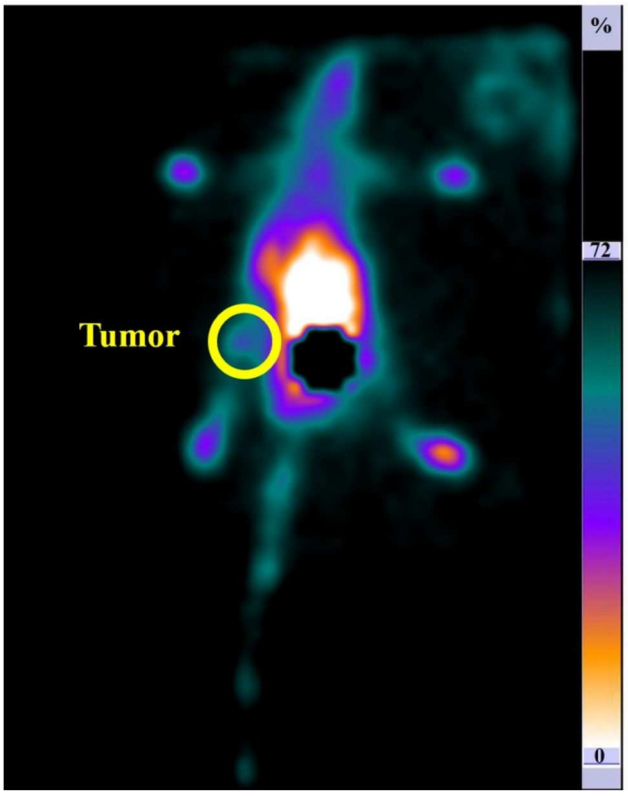

Fig. 9 *Planar images with ^{99m}Tc radiolabelled dendrimer in mice acquired 60 min post-injection: the posterior position. The circle indicates the tumour site. The accumulation of the nanocomplex in the tumour site is apparent in the image*

3.5 Biodistribution results

The biodistribution of radiolabelled folate conjugated dendrimers was measured at 1, 2, and 3 h post-injections.

As shown in Fig. 10, the highest radioactivity was observed at the tumour site due to the implemented targeting approach. Furthermore, the injection dose percent of nanoconjugates was 4.68 ± 0.04% in the kidney 1 h after injection, which decreased to 2.48 ± 0.12% 3 h after injection.

4 Discussion

In this study, we developed PEG-citrate dendrimers decorated with ^{99m}Tc and conjugated with folate as the SPECT contrast agent for MI of breast cancer. This study is the first report on the fabrication of G3 dendrimer composed of PEG and citrate, which radiolabelled

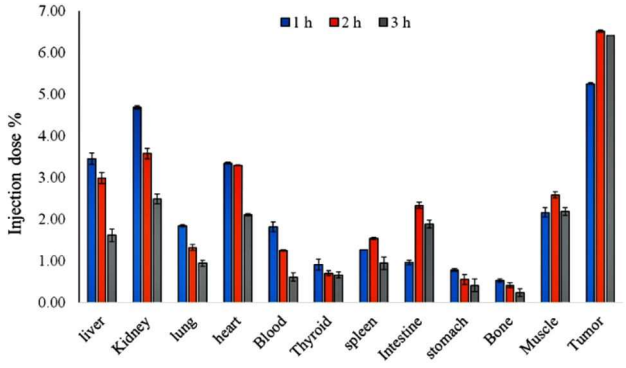

Fig. 10 *Biodistribution profile of nanoconjugate at 1, 2, and 3 time intervals (dose per gram of tissue). The nanocomplexes are accumulated into tumour tissue post-injection at all time points*

with ^{99m}Tc and conjugated with folate as the targeted SPECT contrast agent for early breast cancer detection. In this regard, the DCC conjugation chemistry was used to synthesise and conjugate the PEG-citrate dendrimer and the fabricated dendrimers were characterised via FT-IR, 1H-NMR, LC-MS, DLS, and TEM.

Size evaluations by DLS and TEM demonstrated an increase in the size of dendrimer after conjugation with folic acid, which confirmed the conjugation process. Moreover, reducing the surface charge of dendrimers after conjugation can be an indication of folic acid attachment on the surface of dendrimers, as shown in our previous study [48]. The difference between sizes obtained from TEM imaging and DLS measurement is based on this fact that TEM visualises the particle and hence results in the actual diameter, while DLS measures the hydrated particles, hence the hydrodynamic diameter. We previously reported the size of 91 nm for linear-globular PEG-based dendrimer [51]. Tsutsumi *et al.* [52] synthesised G3 polyamidoamine dendrimer as the small interfering RNA (siRNA) carrier and reported the size range of 136–278 nm for the dendrimer. In another study, Arima *et al.* [53] reported a size range of 290–422 nm for fabricated G3 PAMAM dendrimers. Namazi *et al.* [54] fabricated G1, G2, and G3 dendrimers of citric acid/PEG as the delivery system for naproxen confirmed by FT-IR and ^{1}H NMR spectroscopies and DLS. They reported that the FT-IR and ^{1}H NMR spectroscopies confirmed the formation of dendrimers with the size range of 16–50 nm. The drug load and release studies showed that increasing the generation of dendrimers increased the amount of trapped drugs into the dendrimers.

In vitro stability assessment, up to 24 h revealed that the fabricated dendrimers are stable in the biological media. Filippi *et al.* [55] reported the fabrication of highly stable dendrimers based on Gadoteridol and polyethyleneglycol. They reported the stability of dendrimers in the presence of human serum up to70 h.

XTT toxicity assay showed no cellular toxicity of the synthesised dendrimers. This finding is in line with Namazi *et al.* [54] study that showed the fabricated dendrimers did not elicit significant toxic effects on the cells. Abdoli *et al.* [56] fabricated a multi-epitopic HIV-1 vaccine composed of PEG-citrate G2 dendrimer conjugated with four immunodominant epitopes of the HIV-1 genome. They also used DCC conjugation chemistry for both the synthesis and conjugation. They reported an increase in size and reduction of surface charge after conjugation with peptides. Their toxicity assessment confirmed the biocompatibility of the fabricated dendrimer, which is in agreement with our findings. Naeini *et al.* [57] fabricated triblock copolymers containing PEG and citric acid dendrimer and observed considerable toxicity against human fibrosarcoma (HT1080 cell line), while the dendrimers fabricated in this study were biocompatible.

The biodistribution evaluation of the fabricated dendrimers showed the highest dendrimer accumulation was in the tumour site at 1, 2, and 3 h post-injections. These results confirmed the efficacy of the targeting strategy, which is highly desirable. The observed radioactivity in the kidney implied that the main excretion route of the nanoconjugates is through kidneys, which can be related to the lipophilicity of the fabricated nanocomplex. Moreover, the liver showed a high level of radioactivity uptake at the first-hour post-injection, which can be related to a liver accumulation tendency of the synthesised nanoconjugates. As shown in Fig. 7, the high radioactivity observed in the intestine after 2 h indicates a quick washout through the intestine. Our previous study [48] also indicated that the kidney is the main clearance route of G2-dendrimers of PEG-citric acid. The fabricated dendrimers in this study showed the suitable biodistribution, which was in agreement with our previous work [48] and better than 18F-glutamine [58] dendrimers. The proper biodistribution observed in this study can be attributed to the stability, low molecular weight, and higher solubility of the fabricated dendrimers.

Interestingly, the fabricated dendrimers exhibited a substantial tumour accumulation pattern, which is related to the passive (size of dendrimers) and active (conjugated folic acid) targeting implemented in the dendrimers. The administrated dendrimers can be cleared from the body via the kidney pathway and also participation in the tricarboxylic acid (TCA) cycle in the liver due to the presence of citric acid [48]. Lesniak *et al.* [59] fabricated Cy5-conjugated PAMAM dendrimer and observed accumulation of dendrimer in kidneys and bladder at 24 h, which is in agreement with our observation. In another study, Peng *et al.* [60] fabricated PEGylated dendrimer-entrapped gold nanoparticles as the computed tomography. They administrated the dendrimer via intraperitoneal and intravenous routes and assessed the biodistribution. They observed the highest dendrimer accumulation in the spleen in both injection routes. Accumulation of a high amount of dendrimers in the tumour tissue in our study is related to the active targeting implemented by folate conjugation.

Our findings revealed the valuable prospects of PEG-citrate dendrimers radiolabelled with ^{99m}Tc and conjugated with folic acid, including facile fabrication and conjugation chemistry, biocompatibility, stability in the biological fluids, proper cellular uptake, and bright SPECT signal in vivo. Overall, our results confirmed the potential of the fabricated dendrimers as the SPECT contrast agent for cancer detection. However, more studies need to be done to reveal every aspect of the contrast agent. For instance, the stability of the formulation should be evaluated in a longer time and the fate of the administered nanocomplex should be assed in the body. Moreover, the possibility to formulate a theranostic agent based on the synthesised nanocomplex can be considered.

5 Conclusion

This study aimed to develop a targeted SPECT contrast agent composed of PEG-citrate dendrimer radiolabelled with ^{99m}Tc and conjugated with folic acid for breast cancer detection. Our results revealed that the synthesised dendrimers did not induce significant toxicity and were stable in serum. The imaging studies showed that the dendrimers provided a bright SPECT image after injection into tumour-bearing mice. The biodistribution study confirmed that the dendrimers could accumulate into the tumour, and the kidney is the main clearance route. Our findings revealed the valuable prospects of PEG-citrate dendrimers radiolabelled with ^{99m}Tc and conjugated with folic acid including, facile fabrication and conjugation chemistry, biocompatibility, stability in the biological fluids, proper cellular uptake, and bright SPECT signal in vivo. Overall, our results confirmed the potential of the fabricated dendrimers as the SPECT contrast agent for cancer detection. However, more studies regarding the longtime stability of the nanocomplex in the shelf, as well as its final fate, need to be done to reveal every aspect of the contrast agent.

6 Acknowledgments

This study was supported by Vice Chancellor for Research (grant no. 36365), Tehran University of Medical Sciences, Tehran, Iran. This research did not receive any other grant from funding agencies in the public, commercial, or not-for-profit sectors.

7 References

[1] Peart, O.: 'Breast intervention and breast cancer treatment options', *Radiol. Technol.*, 2015, **86**, (5), pp. 535M–558M

[2] Teles, R.H.G., Moralles, H.F., Cominetti, M.R.: 'Global trends in nanomedicine research on triple negative breast cancer: a bibliometric analysis', *Int. J. Nanomed.*, 2018, **13**, p. 2321

[3] Siegel, R.L., Miller, K.D., Jemal, A.: 'Cancer statistics, 2019', *CA-Cancer J. Clin.*, 2019, **69**, (1), pp. 7–34

[4] Maselli-Schoueri, J.H., Affonso-Kaufman, F.A., de Melo Sette, C.V., *et al.*: 'Time trend of breast cancer mortality in Brazilian men: 10-year data analysis from 2005 to 2015', *BMC Cancer*, 2019, **19**, (1), p. 23

[5] Siegel, R.L., Miller, K.D., Jemal, A.: 'Cancer statistics, 2019', *CA-Cancer J. Clin.*, 2015, **69**, (1), pp. 7–34

[6] Ferrari, M.: 'Cancer nanotechnology: opportunities and challenges', *Nat. Rev. Cancer*, 2005, **5**, (3), p. 161

[7] Farhood, B., Samadian, H., Ghorbani, M., *et al.*: 'Physical, dosimetric and clinical aspects and delivery systems in neutron capture therapy', *Rep. Pract. Oncol. Radiother.*, 2018, **23**, (5), pp. 462–473

[8] Meshkat, M., Baghestani, A.R., Zayeri, F., *et al.*: 'Survival rate and prognostic factors among Iranian breast cancer patients', *Iran J. Public Health*, 2020, **49**, (2), p. 341

[9] Marinovich, M.L., Bernardi, D., Macaskill, P., *et al.*: 'Agreement between digital breast tomosynthesis and pathologic tumour size for staging breast cancer, and comparison with standard mammography', *Breast*, 2019, **43**, pp. 59–66

[10] Hai, J., Tan, H., Chen, J., *et al.*: 'Multi-level features combined End-to-End learning for automated pathological grading of breast cancer on digital mammograms', *Comput. Med. Imaging Graph.*, 2019, **71**, pp. 58–66

[11] Patankar, R.: 'A survey on computer-aided breast cancer detection using mammograms', *Natl. J. Comput. Appl. Sci.*, 2019, **2**, (1), pp. 1–6

[12] Benzebouchi, N.E., Azizi, N., Ayadi, K.: 'A computer-aided diagnosis system for breast cancer using deep convolutional neural networks', in Behera, H.S., Nayak, J., Naik, B., *et al.* (Eds.): '*Computational intelligence in data mining*', (Springer, Switzerland, 2019), pp. 583–593

[13] Hsu, S.-M., Kuo, W.-H., Kuo, F.-C., *et al.*: 'Breast tumor classification using different features of quantitative ultrasound parametric images', *Int. J. Comput. Assist. Radiol. Surg.*, 2019, **14**, pp. 1–11

[14] Pan, Q., Ji, J.: 'Diagnostic value of ultrasound combined with magnetic resonance imaging in different stages of breast cancer', *Oncol. Lett.*, 2019, **17**, (1), pp. 209–214

[15] Tahmassebi, A., Wengert, G.J., Helbich, T.H., *et al.*: 'Impact of machine learning with multiparametric magnetic resonance imaging of the breast for early prediction of response to neoadjuvant chemotherapy and survival outcomes in breast cancer patients', *Invest. Radiol.*, 2019, **54**, (2), pp. 110–117

[16] Yano, F., Itoh, M., Hirakawa, H., *et al.*: 'Diagnostic accuracy of positron emission mammography with 18f-fluorodeoxyglucose in breast cancer tumor of less than 20 Mm in size', *Asia Oceania J. Nucl. Med. Biol.*, 2019, **7**, (1), pp. 13–21

[17] Turkmen, C.: 'Nuclear medicine imaging in breast cancer', in Aydiner, A., Igci, A., Soran, A. (Eds.): '*Breast cancer*', (Springer, Switzerland, 2019), pp. 223–237

[18] Simanek, M., Koranda, P.: 'Spect/Ct imaging in breast cancer-current Status and challenges', *Biomed. Pap. Med. Faculty Palacky Univer. Olomouc*, 2016, **160**, (4), pp. 474–483

[19] Choi, Y.-E., Kwak, J.-W., Park, J.W.: 'Nanotechnology for early cancer detection', *Sensors*, 2010, **10**, (1), pp. 428–455

[20] Avitabile, E., Bedognetti, D., Ciofani, G., *et al.*: 'How can nanotechnology help the fight against breast cancer?', *Nanoscale*, 2018, **10**, pp. 11719–11731

[21] Pysz, M.A., Gambhir, S.S., Willmann, J.K.: 'Molecular imaging: current status and emerging strategies', *Clin. Radiol.*, 2010, **65**, (7), pp. 500–516

[22] Willmann, J.K., Van Bruggen, N., Dinkelborg, L.M., *et al.*: 'Molecular imaging in drug development', *Nat. Rev. Drug Discovery*, 2008, **7**, (7), p. 591

[23] Østergaard, M., Pedersen, S.J., Døhn, U.M.: 'Imaging in rheumatoid arthritis – status and recent advances for magnetic resonance imaging, ultrasonography, computed tomography and conventional radiography', *Best Pract. Res. Clin. Rheumatol.*, 2008, **22**, (6), pp. 1019–1044

[24] Albano, D., Bertagna, F., Giubbini, R.: 'Molecular imaging in the diagnosis of infectious endocarditis – the role of PET and SPECT', *Int. J. Cardiovasc. Sci.*, 2020, **33**, (1), pp. 87–93

[25] Azarnezhad, A., Samadian, H., Jaymand, M., *et al.*: 'Toxicological profile of lipid-based nanostructures: are they considered as completely safe nanocarriers?', *Crit. Rev. Toxicol.*, 2020, **50**, pp. 148–176

[26] Mortezaee, K., Najafi, M., Samadian, H., *et al.*: 'Redox interactions and genotoxicity of metal-based nanoparticles: a comprehensive review', *Chem.-Biol. Interact.*, 2019, **312**, p. 108814

[27] Khoshnevisan, K., Daneshpour, M., Barkhi, M., *et al.*: 'The promising potentials of capped gold nanoparticles for drug delivery systems', *J. Drug Targeting*, 2018, **26**, (7), pp. 525–532

[28] Massoumi, B., Abbasian, M., Jahanban-Esfahlan, R., *et al.*: 'Pegylated hollow Ph-responsive polymeric nanocapsules for controlled drug delivery', Polymer International

[29] Jahanban-Esfahlan, R., Massoumi, B., Abbasian, M., *et al.*: 'Dual stimuli-responsive polymeric hollow nanocapsules as 'smart' drug delivery system against cancer', *Polym.-Plast. Technol. Mater.*, 2020, **59**, pp. 1492–1504

[30] Samadian, H., Maleki, H., Fathollahi, A., *et al.*: 'Naturally occurring biological macromolecules-based hydrogels: potential biomaterials for peripheral nerve regeneration', *Int. J. Biol. Macromol.*, 2020, **154**, pp. 795–817

[31] Samadian, H., Mobasheri, H., Hasanpour, S., *et al.*: 'Electro-conductive carbon nanofibers as the promising interfacial biomaterials for bone tissue engineering', *J. Mol. Liq.*, 2020, **298**, p. 112021

[32] Samadian, H., Vaez, A., Ehterami, A., *et al.*: 'Sciatic nerve regeneration by using collagen type I hydrogel containing naringin', *J. Mater. Sci., Mater. Med.*, 2019, **30**, (9), p. 107

[33] Ehterami, A., Salehi, M., Farzamfar, S., *et al.*: 'A promising wound dressing based on alginate hydrogels containing vitamin D3 cross-linked by calcium carbonate/D-glucono-Δ-lactone', *Biomed. Eng. Lett.*, 2020, **10**, pp. 309–319

[34] Samadian, H., Ehterami, A., Sarrafzadeh, A., *et al.*: 'Sophisticated polycaprolactone/gelatin nanofibrous nerve guided conduit containing platelet-rich plasma and citicoline for peripheral nerve regeneration: in vitro and in vivo study', *Int. J. Biol. Macromol.*, 2020, **150**, pp. 380–388

[35] Khoshnevisan, K., Maleki, H., Samadian, H., *et al.*: 'Antibacterial and antioxidant assessment of cellulose acetate/polycaprolactone nanofibrous mats impregnated with propolis', *Int. J. Biol. Macromol.*, 2019, **140**, pp. 1260–1268

[36] Pillai, G.: 'Nanotechnology toward treating cancer: a comprehensive review', in Mohapatra, S.S., Ranjan, S., Dasgupta, N., *et al.* (Eds.): '*Applications of targeted nano drugs and delivery systems*', (Elsevier, USA., 2019), pp. 221–256

[37] Moloudi, K., Samadian, H., Jaymand, M., *et al.*: 'Iron oxide/gold nanoparticles-decorated reduced graphene oxide nanohybrid as the thermo-radiotherapy agent', *IET Nanobiotechnol.*, 2020, **14**, pp. 428–432

[38] Svenson, S., Tomalia, D.A.: 'Dendrimers in biomedical applications – reflections on the field', *Adv. Drug Deliv. Rev.*, 2012, **64**, pp. 102–115

[39] Mohammadzadeh, P., Ardestani, M.S., Mortazavi-Derazkola, S., *et al.*: 'Peg-citrate dendrimer second generation: is this a good carrier for imaging agents in vitro and in vivo?', *IET Nanobiotechnol.*, 2019, **13**, (6), pp. 560–564

[40] Abolghasemi, M.M., Habibiyan, R., Jaymand, M., *et al.*: 'A star-shaped polythiophene dendrimer coating for solid-phase microextraction of triazole agrochemicals', *Microchim. Acta*, 2018, **185**, (3), p. 179

[41] Villaverde, A.: '*Nanoparticles in translational science and medicine*' (Academic Press, Germany, 2011)

[42] Namazi, H., Adeli, M.: 'Dendrimers of citric acid and poly (ethylene glycol) as the new drug-delivery agents', *Biomaterials*, 2005, **26**, (10), pp. 1175–1183

[43] Namazi, H., Adeli, M.: 'Novel linear–globular thermoreversible hydrogel aba type copolymers from dendritic citric acid as the A blocks and poly (ethyleneglycol) as the B block', *Eur. Polym. J.*, 2003, **39**, (7), pp. 1491–1500

[44] Ebrahimi, S., Sadeghizadeh, M., Aghasadeghi, M., *et al.*: 'One-step synthesis of anionic peg-citrate G2 dendrimer and evaluation of its cytotoxicity in two cell lines', *Pathobiol. Res.*, 2015, **17**, (4), pp. 13–24

[45] Meier, R., Henning, T.D., Boddington, S., *et al.*: 'Breast cancers: mr Imaging of folate-receptor expression with the folate-specific nanoparticle P1133', *Radiology*, 2010, **255**, (2), pp. 527–535

[46] Necela, B.M., Crozier, J.A., Andorfer, C.A., *et al.*: 'Folate receptor-A (Folr1) expression and function in triple negative tumors', *PloS One*, 2015, **10**, (3), p. e0122209

[47] Fisher, R.E., Siegel, B.A., Edell, S.L., *et al.*: 'Exploratory study of 99mtc-Ec20 imaging for identifying patients with folate receptor-positive solid tumors', *J. Nucl. Med.*, 2008, **49**, (6), p. 899

[48] Ghoreishi, S.M., Khalaj, A., Sabzevari, O., *et al.*: 'Technetium-99 m chelator-free radiolabeling of specific glutamine tumor imaging nanoprobe: in vitro and in vivo evaluations', *Int. J. Nanomed.*, 2018, **13**, p. 4671

[49] Liu, X., Liu, J., Guan, Y., *et al.*: 'Establishment of an orthotopic lung cancer model in nude mice and its evaluation by spiral Ct', *J. Thorac. Dis.*, 2012, **4**, (2), p. 141

[50] Chandrasekar, D., Sistla, R., Ahmad, F.J., *et al.*: 'Folate coupled poly (ethylene glycol) conjugates of anionic poly (amidoamine) dendrimer for inflammatory tissue specific drug delivery', *J. Biomed. Mater. Res. A*, 2007, **82**, (1), pp. 92–103

[51] Assadi, A., Najafabadi, V.S., Shandiz, S.A.S., *et al.*: 'Novel chlorambucil-conjugated anionic linear-globular peg-based second-generation dendrimer: in vitro/in vivo improved anticancer activity', *Onco. Targets Ther.*, 2016, **9**, p. 5531

[52] Tsutsumi, T., Hirayama, F., Uekama, K., *et al.*: 'Evaluation of polyamidoamine dendrimer/A-cyclodextrin conjugate (generation 3, G3) as a novel carrier for small interfering rna (sirna)', *J. Controlled Release*, 2007, **119**, (3), pp. 349–359

[53] Arima, H., Chihara, Y., Arizono, M., *et al.*: 'Enhancement of gene transfer activity mediated by mannosylated dendrimer/A-cyclodextrin conjugate (generation 3, G3)', *J. Controlled Release*, 2006, **116**, (1), pp. 64–74

[54] Namazi, H., Motamedi, S., Namvari, M.: 'Synthesis of new functionalized citric acid-based dendrimers as nanocarrier agents for drug delivery', *Bioimpacts*, 2011, **1**, (1), p. 63

[55] Filippi, M., Patrucco, D., Martinelli, J., *et al.*: 'Novel stable dendrimersome formulation for safe bioimaging applications', *Nanoscale*, 2015, **7**, (30), pp. 12943–12954

[56] Abdoli, A., Radmehr, N., Bolhassani, A., *et al.*: 'Conjugated anionic peg-citrate G2 dendrimer with multi-epitopic HIV-1 vaccine candidate enhance the cellular immune responses in mice', *Artif. Cells Nanomed. Biotechnol.*, 2017, **45**, (8), pp. 1762–1768

[57] Naeini, A.T., Adeli, M., Vossoughi, M.: 'Poly (citric acid)-block-poly (ethylene glycol) copolymers – new biocompatible hybrid materials for nanomedicine', *Nanomed. Nanotechnol. Biol. Med.*, 2010, **6**, (4), pp. 556–562

[58] Ploessl, K., Wang, L., Lieberman, B.P., *et al.*: 'Comparative evaluation of 18f-labeled glutamic acid and glutamine as tumor metabolic imaging agents', *J. Nucl. Med.*, 2012, **53**, (10), pp. 1616–1624

[59] Lesniak, W.G., Mishra, M.K., Jyoti, A., *et al.*: 'Biodistribution of fluorescently labeled pamam dendrimers in neonatal rabbits: effect of neuroinflammation', *Mol. Pharm.*, 2013, **10**, (12), pp. 4560–4571

[60] Peng, C., Zheng, L., Chen, Q., *et al.*: 'Pegylated dendrimer-entrapped gold nanoparticles for in vivo blood pool and tumor imaging by computed tomography', *Biomaterials*, 2012, **33**, (4), pp. 1107–1119